

Article

A Novel Optimization Strategy of Bearing Geometry with a Length to Diameter Ratio of 1.25 under Severe Operating Conditions Using Taguchi Method

Hazim U. Jamali ¹ , M. N. Mohammed ² , H. S. S. Aljibori ³, Muhsin Jaber Jweeg ⁴ and Oday I. Abdullah ^{5,2,6,*} 

¹ Mechanical Engineering Department, College of Engineering, University of Kerbala, Karbala 56001, Iraq; hazimumran@uokerbala.edu.iq

² Mechanical Engineering Department, College of Engineering, Gulf University, Sanad 26489, Bahrain; dr.mohammed.alshekhly@gulfuniversity.edu.bh

³ Al-Warath Center for Crowd Engineering and Management Research, University of Warith Al-Anbiyaa, Karbala 56001, Iraq; hakim.s@uowa.edu.iq

⁴ College of Technical Engineering, Al-Farahidi University, Baghdad 00965, Iraq; muhsin.jweeg@uoalfarahidi.edu.iq

⁵ Department of Energy Engineering, College of Engineering, University of Baghdad, Baghdad 10071, Iraq

⁶ Department of Mechanics, Al-Farabi Kazakh National University, Almaty 050040, Kazakhstan

* Correspondence: oday.abdullah@tuhh.de

Abstract: Robust and well-designed rotor-bearing systems ensure safe operation and a high level of reliability under severe operating conditions. A deviation in the shaft axis with respect to the bearing longitudinal axis represents one of the most unavoidable problems in bearing systems. This deviation results from installation errors, manufacturing errors, shaft deformation under heavy loads, bearing wear, and many other causes. Each of these deviation sources has its negative consequences on the designed characteristics of the system. This work deals with the geometrical design of a journal bearing using three forms of profiles (linear ($n = 1$), quadratic ($n = 2$) and cubic ($n = 3$) profiles) in order to enhance bearing performance despite the presence of the inevitable shaft deviation. In addition, a wide range of bearing profile parameters are considered in the analysis to optimize the bearing profile based on the use of the Taguchi method. A general form of shaft deviation is considered to account for both horizontal and vertical deviations. A numerical solution is obtained using the finite difference method. The results show that all three suggested forms of bearing profiles elevate the film thickness significantly and also reduce the friction coefficient, but with different effects on the maximum pressure values. The Taguchi method illustrates that the optimal geometrical design parameters are the quadratic profile and the modification of one-fifth of the bearing width from both sides at a height of just less than half the radial clearance ($0.4 C$) at the bearing edges. These values give the best combination of the considered main bearing characteristics: the minimum film thickness, coefficient of friction, and maximum pressure. The results show that the minimum film thickness is increased by 184%, the maximum pressure is reduced by 15.1% and the friction coefficient is decreased by 6.4% due to the use of the suggested design. The outcome of this work represents an important enhancement step for the rotor bearing performance to work safely with high reliability under severe shaft deviation levels. This can be implied at the design stage of the bearing, which requires prior knowledge about the operating conditions in order to have better estimation for the levels of shaft deviation.

Keywords: Taguchi method; friction; misalignment; geometrical design



Citation: Jamali, H.U.; Mohammed, M.N.; Aljibori, H.S.S.; Jweeg, M.J.; Abdullah, O.I. A Novel Optimization Strategy of Bearing Geometry with a Length to Diameter Ratio of 1.25 under Severe Operating Conditions Using Taguchi Method. *Designs* **2023**, *7*, 121. <https://doi.org/10.3390/designs7060121>

Received: 27 September 2023

Revised: 16 October 2023

Accepted: 23 October 2023

Published: 26 October 2023



Copyright: © 2023 by the authors. Licensee MDPI, Basel, Switzerland. This article is an open access article distributed under the terms and conditions of the Creative Commons Attribution (CC BY) license (<https://creativecommons.org/licenses/by/4.0/>).

1. Introduction

Hydrodynamic journal bearing is a significant type of bearing which represents a core component in turbines, generators, pumps, and many types of machinery used in industrial applications [1]. This type of bearing is characterized by several features, such

as high reliability, relatively low noise levels, and stable operation [2]. It is widely used in high-speed and heavy-loaded rotating machinery [3]. However, its performance can be affected by many factors, such as poor operating conditions, manufacturing errors, misalignment, and even long service times. These factors and many others may lead to the failure of the journal bearing or, at least, reduce efficiency, affecting machinery reliability [2]. The rotation of the shaft inside the bearing takes place within a clearance filled with a relevant lubricant, in the order of tens of microns. Therefore, this thin gap provides relatively limited tolerance for any deviation from parallelism between the longitudinal axes of these two components. This deviation is usually called misalignment, which is one of the most unavoidable problems in journal bearings that has severe negative impacts on the rotor-bearing system [4,5]. Misalignment results due to a wide range of causes, such as installation errors, deformation under high loads, bearing wear, and asymmetric loading [6–8]. Misalignment in the shaft axis with respect to the bearing's longitudinal axis results in asymmetric pressure distribution, deviating the point of equivalent support away from the midplane of the bearing width [9,10]. This asymmetry results in negative consequences for pressure, friction, and film thickness levels. Extensive work has been performed to investigate the misalignment effects on the performance of this type of bearing. Jang and Khonsari [11] examined the impact of misalignment on the characteristics of journal bearing. The relationship between load-carrying capacity and misalignment was investigated by Pigott [12], where it was found that a significant reduction in this designed parameter resulted due to the problem of misalignment. Similar results regarding the drop in film thickness and load-carrying capacity due to misalignment have also been reported by [13,14]. Severe thinning of the lubricant as a result of misalignment may lead to metal-to-metal contact, which may cause failure in the rotor-bearing system [15,16]. Furthermore, friction also increases due to misalignment at the most affected position along the bearing width [17]. Misalignment also has an obvious relation with bearing wear [18–20]. Wear and friction problems have been investigated over the last few decades due to their impact on the performance as well as the lifespan of the rotor-bearing system [21,22]. Dufrane et al. [22] showed in their model of wear in hydrodynamic lubrication that there is a certain film thickness limit in relation to the development of wear. Nikolakopoulos and Papadoulos [16] proposed a model for the hydrodynamic lubrication of journal bearings to find relationships among the friction coefficient, wear, and the level of misalignment for a range of Sommerfeld numbers.

Many studies have been conducted to reduce the impacts of misalignment on the performance of journal bearings [23]. One of the methods is changing the bearing profile, such as the experimental work of Nacy [24], where side leakage was controlled by chamfering the bearing edges. Another example was the use of predesigned defects in the bearing geometry by Fillon and Bouyer [25] to enhance bearing characteristics under misalignment torque. Chasalevris and Dohnal [26] suggested using variable bearing geometry to improve the system's dynamic behavior. Ren et al. [27] recently used a quadratic bearing profile in a numerical solution to improve bearing performance. Researchers have attempted to evaluate the impact of varying the bearing geometry on its performance, such as [28–32]. However, these studies did not use any optimization strategy, and they investigated limited forms of modifications.

Using a variable profile in designing the journal bearing is based on several parameters, such as the order of the profile, starting position, and height of modification. Every parameter has an impact on the characteristics of the system. Therefore, statistical methods represent an essential step in gathering and evaluating the effects of these parameters in an efficient procedure. The Taguchi method represents an efficient method in this context [33]. The Taguchi method was suggested by Genichi Taguchi in order to reduce the number of tests required in a process of optimization. Yücel and Saruhan [34] used this method to identify the minimum vibration amplitude of rotor-bearing systems, where their solution was found efficient in avoiding operation at critical speeds. Chien et al. [35] used this method in order to calculate the optimum groove design parameters in journal bearings.

They found that using this method enabled the design to have minimum side leakage and also maximum load-carrying capacity. Sharma et al. [36] also used this method to determine the optimal pressure and speed values in an experimental study of a journal bearing made of cast lead bronze material.

Chen et al. [37] used this method to investigate the performance of asymmetrical herringbone grooves in journal bearings. Bhasker et al. [38] used the Taguchi method as an optimization method to determine the optimal parameters for the assessment of pressure distribution. Ganesha et al. [33] also adopted this method to optimize multi-groove journal bearings lubricated with water. Several parameters were considered in their statistical study, such as the attitude angle, height of the groove, and the number of grooves.

Although extensive research has been carried out to enhance journal bearing performance, the problem of shaft deviation, due to several causes such as large shaft deformation and installation errors, still negatively impacts the performance of the system. Therefore, this study presents a novel method to minimize the consequences of this problem by improving bearing design. This work aims to use the Taguchi method in order to optimize the bearing profile under severe levels of misalignment. Three different modification forms are investigated in this novel strategy for the geometrical design of the bearing profile. The bearing is modified using a linear, quadratic, or cubic profile on both sides of the bearing width, with a wide range of height and position modifications. The finite difference method is considered in this work, along with the iterative solution of the Reynolds boundary condition method to determine the boundaries of the cavitation zone. The optimization method considers the combined effect of the studied parameters on the friction coefficient, maximum pressure, and minimum film thickness in finite-length journal bearings.

2. Governing Equations

Figure 1 illustrates an exaggerated scale for a side view of a typical journal bearing in perfectly aligned cases, where the cross-section at any position along the bearing length is the same. In this rarely encountered case in industrial uses of this type of bearing, there is no deviation between the shaft and bearing longitudinal axes. The ideal parallelism between these axes results in the gap given by Equation (1) between the inner surface of the bearing and the journal surface. This equation is used together with the well-known Reynolds Equation (2) to solve the hydrodynamic lubrication problems in this type of bearings [5,39].

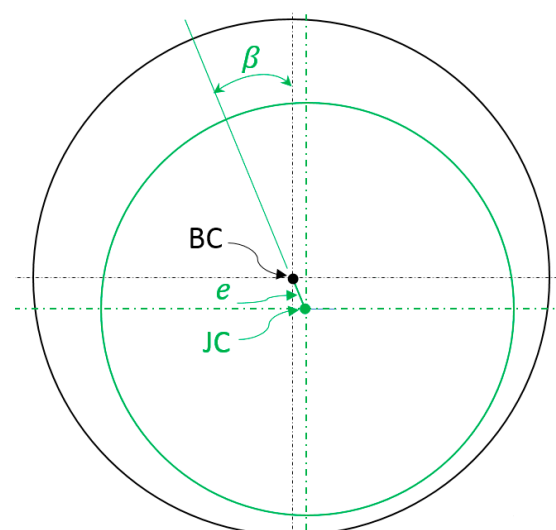


Figure 1. Side view of an aligned journal bearing (an exaggerated scale). (BC: bearing center, JC: journal center).

$$h = c(1 + \epsilon_r \cos(\theta - \beta)) \tag{1}$$

$$\frac{\partial}{\partial x} \left(\frac{\rho h^3}{12\eta} \frac{\partial p}{\partial x} \right) + \frac{\partial}{\partial z} \left(\frac{\rho h^3}{12\eta} \frac{\partial p}{\partial z} \right) = U_m \frac{\partial \rho h}{\partial x} \tag{2}$$

where

h : film thickness.

c : radial clearance.

ϵ_r (e/c): eccentricity ratio (e is the distance between the centers of the journal and the bearing).

β : attitude angle.

θ : position angle

p : pressure.

ρ, η : density and viscosity of the lubricant.

U_m : mean velocity.

The solution of this partial differential Equation (2) is achieved using the Reynolds boundary conditions method. In this method, the following conditions have to be satisfied [40]:

- The value of the pressure, $p = 0$ at $\theta = 0$.
- The value of the pressure and the pressure gradient, $p = \frac{\partial p}{\partial \theta} = 0$ at $\theta = \theta_{cav}$.

where θ_{cav} is the boundary of the cavitation zone, which is identified in this work by an iterative method [40,41]. It is worth mentioning that there is another cavitation algorithm, presented by Vijayaraghavan and Keith [42], which can accurately predict film rupture and reformation in the bearing. However, the Reynolds boundary condition is used in this work to ensure relatively faster convergence, as this work is focused on the design of the bearing profile. The other method will be addressed in future work.

The solution model presented in this work is written in a dimensionless form, using the following relations, $x = R\theta, Z = \frac{z}{L}, H = \frac{h}{c}$ and $P = \frac{p - p_0}{6\eta\omega} \left(\frac{c}{R} \right)^2$.

Using these relations, the previous Equations (1) and (2) are given by

$$H = 1 + \epsilon_r \cos(\theta - \beta) \tag{3}$$

$$\frac{\partial}{\partial \theta} \left(H^3 \frac{\partial P}{\partial \theta} \right) + \alpha \frac{\partial}{\partial Z} \left(H^3 \frac{\partial P}{\partial Z} \right) - \frac{\partial H}{\partial \theta} = 0 \tag{4}$$

where $\alpha = \frac{1}{4(L/D)^2} = \frac{R^2}{L^2}$.

The load supported by the journal bearing in a dimensionless form ($\bar{W} = \frac{w}{6\eta\omega RL} \left(\frac{c}{R} \right)^2$) is

$$\bar{W} = \sqrt{\bar{W}_r^2 + \bar{W}_t^2} \tag{5}$$

where

$$\bar{W}_r = \int_0^1 \int_0^{\theta_{cav}} P \cos \theta \, d\theta \, dz \tag{6}$$

$$\bar{W}_t = \int_0^1 \int_0^{\theta_{cav}} P \sin \theta \, d\theta \, dz \tag{7}$$

The attitude angle can be calculated after determining the load components, as follows [43]

$$\beta = \tan^{-1} \left(\frac{W_t}{W_r} \right) \tag{8}$$

In the current study, the coefficient of friction is also considered to examine the effect of the varying bearing profile on this important contact characteristic. The model of friction used by Lund and Thomsen [44] is considered, which is given by the following:

$$f = \mathcal{F}/W \tag{9}$$

where

$$\mathcal{F} = \bar{\delta}/u;$$

$$\bar{\delta} = \omega \sum \left[\eta R^3 \omega \int_0^\theta l \frac{d\theta}{h} + \frac{1}{2} \varepsilon_r (F_X \sin \beta - F_Y \cos \beta) \right];$$

$$u = R\omega;$$

W : total load;

\mathcal{F} : friction force;

$\bar{\delta}$: power loss;

F_X, F_Y : bearing forces in both directions (these forces are determined using numerical integration).

2.1. Misalignment Model

Figure 2 illustrates the general misalignment model used in this work, which deals with the deviations between the shaft and the bearing axes in both horizontal and vertical directions. This 3D modeling of the deviations represents a comprehensive description of misalignment, which is essentially adopted from a previous study [5]. The main relations used in this model are given by

$$\begin{aligned} \Delta v(Z) &= \Delta v_o(1 - 2Z) \text{ for } Z \leq 1/2 \\ \Delta v(Z) &= \Delta v_o(2Z - 1) \text{ for } Z > 1/2 \\ \Delta h(Z) &= \Delta h_o(1 - 2Z) \text{ for } Z \leq 1/2 \\ \Delta h(Z) &= \Delta h_o(2Z - 1) \text{ for } Z > 1/2 \end{aligned} \tag{10}$$

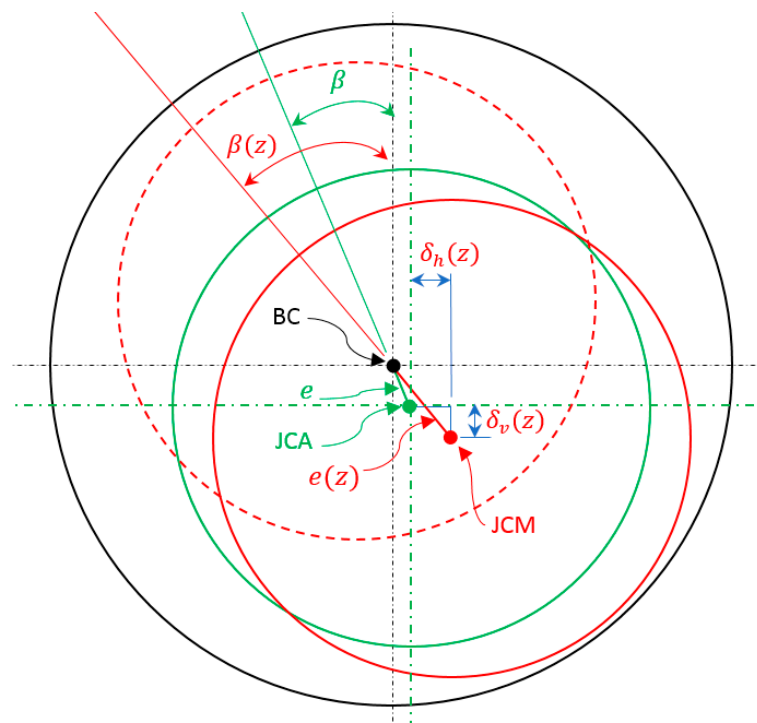


Figure 2. An exaggerated scale of the adopted general misalignment model. Circle in solid red: front side of the misaligned journal, circle in dashed red: rear side of the misaligned journal, and circle in green: journal in its perfectly aligned case. (BC: bearing center, JCA: journal center for the aligned case, and JCM: journal center (front side) for the misaligned case).

The expressions in Equation (10) are also given in their dimensionless forms in order to be consistent with the other equations in this study, where the dimensionless deviation is $\Delta = \delta/c$ and the dimensionless length is $Z = z/L$. This method of modeling gives a more realistic description of the vertical ($\Delta v(z)$) and horizontal ($\Delta h(z)$) deviations of the journal with respect to the longitudinal bearing axis. These deviations are determined in terms of the Z position and the maximum horizontal (Δh_0) and vertical (Δv_0) deviations at the bearing edges.

In ideal aligned journal bearings, the attitude angle as well as the eccentricity between the shaft and the bush centers are constant along the bearing length, which is not the case when misalignment occurs. Their values vary in accordance with the Z position as follows [5]:

$$\begin{aligned} \beta(z) &= \tan^{-1} \frac{e_m \sin \beta_m + \delta h(z)}{e_m \cos \beta_m - \delta v(z)} \text{ when } z \leq L/2 \\ e(z) &= \sqrt{(e_m \cos \beta_m - \delta v(z))^2 + (e_m \sin \beta_m + \delta h(z))^2} \\ \beta(z) &= \tan^{-1} \frac{e_m \sin \beta_m - \delta h(z)}{e_m \cos \beta_m + \delta v(z)} \text{ when } z > L/2 \\ e(z) &= \sqrt{(e_m \cos \beta_m + \delta v(z))^2 + (e_m \sin \beta_m - \delta h(z))^2} \end{aligned} \tag{11}$$

where

β_m : attitude angle at the middle of the bearing length ($z = L/2$).

e_m : eccentricity at $z = L/2$.

Equations (10) and (11), in addition to Equation (3), can be used to determine the gap resulting from misalignment at any z position.

2.2. Variation in the Bearing Profile

It is well known that misalignment results in a severe reduction in the gap at the bearing edges as a result of the slope of the shaft (shaft deviations) with respect to the axis of the bearing. This reduction in the film thickness of the lubricant can be overcome to a large extent by using a variable bearing profile. Figure 3 illustrates the suggested design profiles, with Figure 3a showing the whole bearing with an edge chamfer in a linear form. Changing the bearing profile in this way causes a discontinuity in the slope at the start position of the chamfering. Figure 3b shows three forms of bearing profiles: linear, parabolic, and cubic profiles. The linear profile is the profile mentioned previously in the illustration of Figure 3a. The use of parabolic and cubic profiles ensures slope continuity between the unmodified and modified bearing profiles at the starting position of modification. However, the heights of the two curves are different except at the beginning and the ends of the two profiles. These differences among the three forms will be investigated in detail in this work to identify the optimal bearing profile that reduces the negative effects of misalignment.

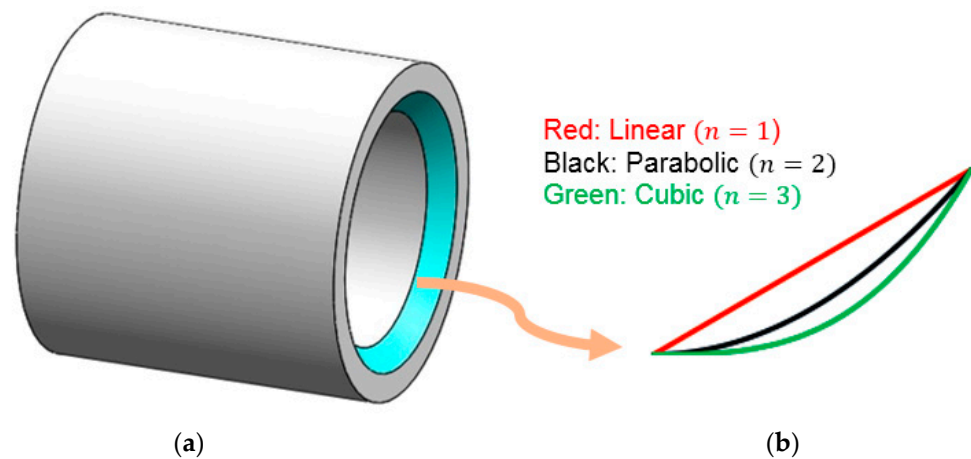


Figure 3. Suggested design of the bearing in an exaggerated scale. (a) Bearing with linear chamfer and (b) three profiles of the bearing edge modification.

These three forms can be represented mathematically using the following general equation:

$$\gamma(z) = (a_0 + a_1z)^n \tag{12}$$

where

$\gamma(z)$: amount of modification in the radial direction in terms of z position along the bearing width (see Figure 4 for the z -axis).

a_0 and a_1 : constants that will be determined later.

n : the order of the equation where $n = 1, 2,$ and 3 represents the linear, parabolic, and cubic profiles, respectively.

Figure 4 shows a longitudinal section of the bearing, with an exaggerated scale of the resulting bearing edges due to the suggested modifications. The three types of profiles are shown together for illustrative purposes. The modification parameters are shown in this figure, which are m_r and m_l , representing the modification's value at the bearing edge in the radial direction and the length of the modified portion from the bearing length on both sides, respectively.

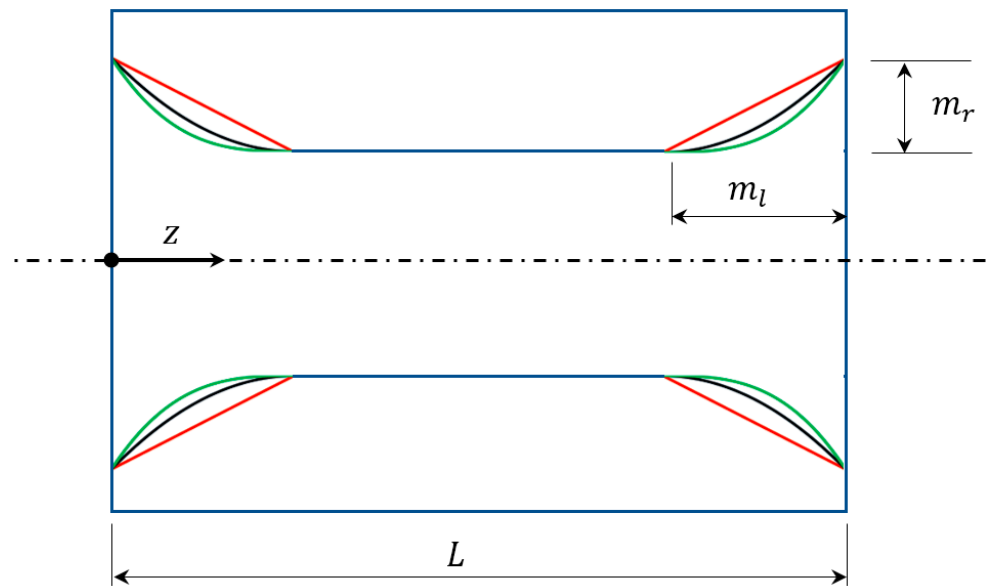


Figure 4. Longitudinal section of the bearing showing an exaggerated scale of the resulting bearing edges.

Regarding these parameters, the constants in Equation (12) for the considered range of n are determined using the following boundary conditions:

- Linear profile ($n = 1$)
 - when $z \leq m_l$:
 - $\gamma(z) = m_r$ at $z = 0$
 - $\gamma(z) = 0$ at $z = m_l$
 - when $z \geq L - m_l$:
 - $\gamma(z) = 0$ at $z = L - m_l$
 - $\gamma(z) = m_r$ at $z = L$
 - when $m_l < z < L - m_l$: $\gamma(z) = 0$
- Parabolic profile ($n = 2$)
 - when $z \leq m_l$:
 - $\gamma(z) = m_r$ at $z = 0$
 - $\gamma(z) = \frac{d\gamma(z)}{dz} = 0$ at $z = m_l$
 - when $z \geq L - m_l$:

$$\begin{aligned} \gamma(z) &= \frac{d\gamma(z)}{dz} = 0 \text{ at } z = L - m_l \\ \gamma(z) &= m_r \text{ at } z = L \\ \text{when } m_l < z < L - m_l: \gamma(z) &= 0 \end{aligned}$$

- Cubic profile ($n = 3$)

$$\begin{aligned} \text{when } z \leq m_l: \\ \gamma(z) &= m_r \text{ at } z = 0 \\ \gamma(z) &= \frac{d\gamma(z)}{dz} = 0 \text{ at } z = m_l \\ \text{when } z \geq L - m_l: \\ \gamma(z) &= \frac{d\gamma(z)}{dz} = 0 \text{ at } z = L - m_l \\ \gamma(z) &= m_r \text{ at } z = L \\ \text{when } m_l < z < L - m_l: \gamma(z) &= 0 \end{aligned}$$

Substituting these boundary conditions into Equation (12) with the use of the corresponding n value results in all the required constant equations, which are shown in Table 1.

Table 1. Equations of the constants a_0 and a_1 for the different values of n .

	$n=1$		$n=2$		$n=3$	
	$z \leq m_l$	$z \geq L - m_l$	$z \leq m_l$	$z \geq L - m_l$	$z \leq m_l$	$z \geq L - m_l$
a_0	m_r	$\frac{-m_r}{m_l}(L - m_l)$	$\sqrt{m_r}$	$\frac{-\sqrt{m_r}}{m_l}(L - m_l)$	$\sqrt[3]{m_r}$	$\frac{-\sqrt[3]{m_r}}{m_l}(L - m_l)$
a_1	$\frac{-m_r}{m_l}$	$\frac{m_r}{m_l}$	$\frac{-\sqrt{m_r}}{m_l}$	$\frac{\sqrt{m_r}}{m_l}$	$\frac{-\sqrt[3]{m_r}}{m_l}$	$\frac{\sqrt[3]{m_r}}{m_l}$

The previous equations relating to the bearing profile can be written in the following dimensionless forms in consistency with the other equations in the current model for the purpose of generality of the results:

- $n = 1:$

$$\begin{aligned} \Gamma(Z) &= \xi(1 - Z/\psi) \text{ when } Z \leq \psi \\ \Gamma(Z) &= \frac{\xi}{\psi}(\psi - 1 + Z) \text{ when } Z \geq 1 - \psi \\ \Gamma(Z) &= 0 \text{ when } \psi < Z < 1 - \psi \end{aligned} \tag{13}$$

- $n = 2:$

$$\begin{aligned} \Gamma(Z) &= \xi(1 - Z/\psi)^2 \text{ when } Z \leq \psi \\ \Gamma(Z) &= \frac{\xi}{\psi^2}(\psi - 1 + Z)^2 \text{ when } Z \geq 1 - \psi \\ \Gamma(Z) &= 0 \text{ when } \psi < Z < 1 - \psi \end{aligned} \tag{14}$$

- $n = 3:$

$$\begin{aligned} \Gamma(Z) &= \xi(1 - Z/\psi)^3 \text{ when } Z \leq \psi \\ \Gamma(Z) &= \frac{\xi}{\psi^3}(\psi - 1 + Z)^3 \text{ when } Z \geq 1 - \psi \\ \Gamma(Z) &= 0 \text{ when } \psi < Z < 1 - \psi \end{aligned} \tag{15}$$

where the dimensionless variables are given by

$$Z = z/L, \Gamma(Z) = \lambda(z)/C, \xi = m_r/C, \text{ and } \psi = m_l/L.$$

The dimensionless Z position ranges from 0 to 1 as z ranges from 0 to L . Scaling the dimensions of the modification to the radial clearance ($\xi = m_r/C$) and the bearing length ($\psi = m_l/L$) gives a much clearer understanding of the amount of required design variations in terms of these two main journal bearing geometry parameters, which are required to compensate for the thinning of the film thickness.

Regarding the determination of the film thickness in the hydrodynamic problem of the journal bearing, while considering the profile variation and misalignment effects, the total gap is calculated through the coupling of the related Equations (3), (10), (11), and (13)–(15).

3. Numerical Solution and the Taguchi Method

The current problem is solved numerically, taking into account the shaft misalignment effects and the variation in the bearing profile. The governing equations are discretized using the finite difference method. The resulting equations are solved using the Gauss–Seidel method, considering a successive over-relaxation solution in order to determine the film thickness, pressure field, and coefficient of friction. The Gauss–Seidel method, which is an iterative method, provides efficient control over round-off errors, and more importantly, if the problem physics are well-known, the convergence becomes faster by selecting relevant initial guesses based on these physics. The discretization scheme results in the following equations, and the required results are obtained based on an iterative solution of these equations:

$$P_{(i,j)} = \frac{1}{\chi} \left[H_b^3 P_{(i+1,j)} + H_a^3 P_{(i-1,j)} + \alpha C_2 H_c^3 P_{(i,j+1)} + \alpha C_2 H_d^3 P_{(i,j-1)} - C_1 H_{(i+1,j)} + C_1 H_{(i-1,j)} \right] \tag{16}$$

$$H(i, j) = \left(1 + \varepsilon_r(Z) \cos(\theta_{(i,j)} - \beta) \right) \tag{17}$$

where

$C_1 = 0.5 \Delta\theta$, $C_2 = (\Delta\theta/\Delta Z)^2$, $\chi = H_b^3 + H_a^3 + \alpha C_2 H_c^3 + \alpha C_2 H_d^3$ and $\Delta\theta$, ΔZ are the step sizes (circumferential direction step and longitudinal direction step, respectively).

A full description of the solution procedure as well as the discretization scheme are explained in detail in reference [5].

The solution of this hydrodynamic problem is performed using a pressure convergence criterion that is given by

$$\frac{\sum_{j=1}^M \sum_{i=1}^N |P_{(i,j)_{new}} - P_{(i,j)_{old}}|}{\sum_{j=1}^M \sum_{i=1}^N P_{(i,j)_{old}}} < 10^{-7} \tag{18}$$

where M and N represent the number of nodes in the circumzenithal and longitudinal directions, respectively. Once the solution converges in terms of the pressure distribution, the load is determined by integrating the pressure field numerically. The resulting load from this integration must be within an accuracy limit of $\pm 10^{-5}$ in comparison to the real supported load. Otherwise, ε_r is changed, and all the previous steps are repeated again in order to obtain a new pressure field. This process continues until both convergence criteria are satisfied. Then, the optimization process is started using the Taguchi method to identify the optimal bearing profile in terms of the profile order (n), and the profile parameters ζ and ψ . Figure 5 illustrates these solution steps. It is worth mentioning that the load in all cases corresponds to the load of the aligned case when the eccentricity ratio is 0.6.

The complete solution to this hydrodynamic problem requires considering other important aspects, such as thermal and bearing deformation effects. An increase in lubricant temperature reduces its viscosity, which leads to a reduction in film thickness under the same applied load. Bearing deformation, on the other hand, changes its geometry and affects the distribution of pressure and film thickness. However, an accurate consideration of these effects requires the solution of energy equations and an elasto-hydrodynamic solution. These aspects will be addressed in future work, as this study is focused on bearing geometry design.

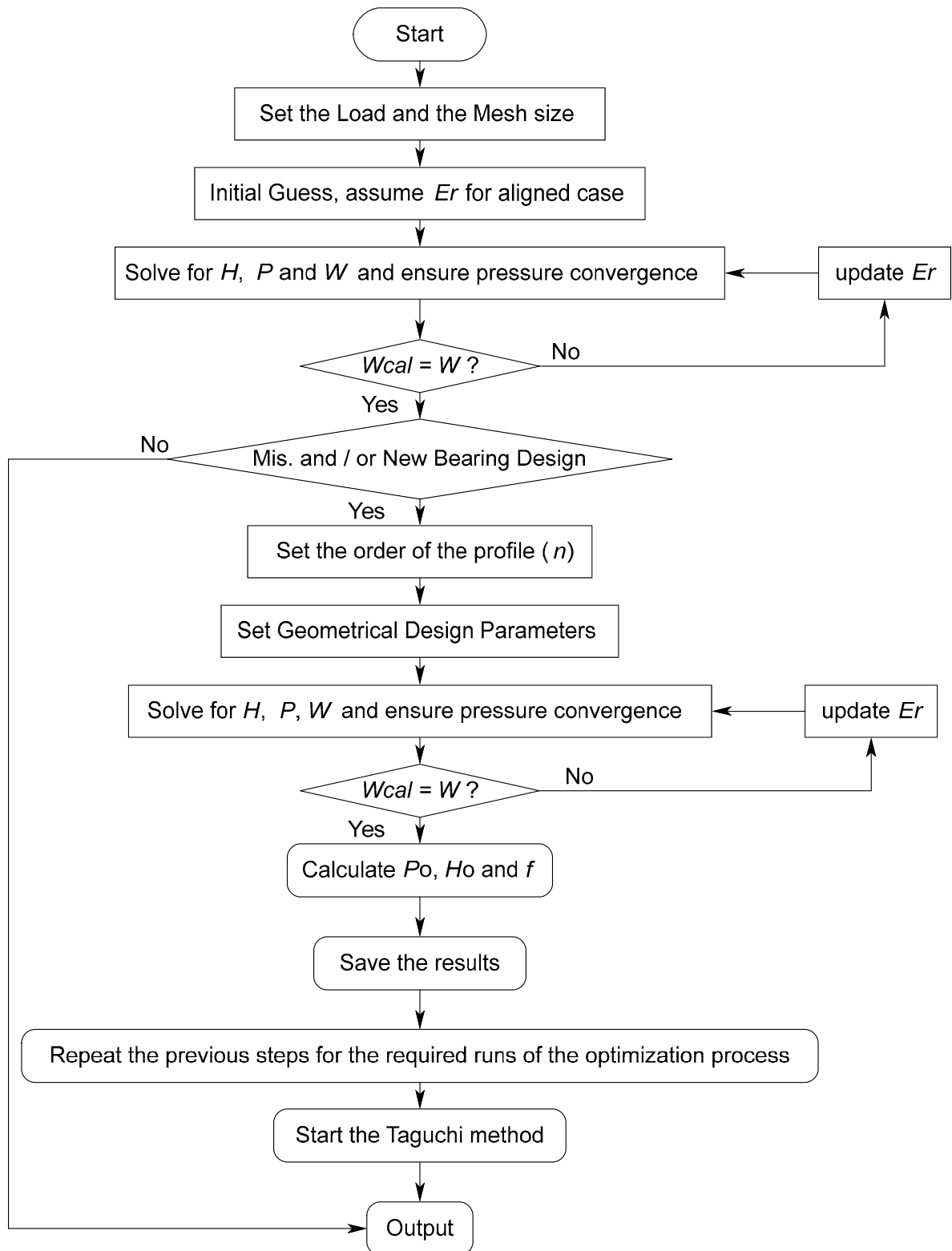


Figure 5. Solution steps of the problem.

4. Results and Discussion

This work presents the results for a finite-length misaligned journal bearing, considering bearing profile modifications in addition to the use of the Taguchi method in order to optimize the bearing profile. The length-to-diameter ratio for this finite-length bearing is 1.25, requiring the numerical solution to consider pressure gradients in both directions of the solution space. In this numerical solution, a series of tests are performed to ensure the independence of the results from the number of nodes, with 65,341 nodes considered. A much lower number is found sufficient, as increasing the number of nodes only produces a trivial variation in the friction coefficient. However, the considered number is adopted in order to minimize any possible errors relating to number of nodes. All the results in this work are presented in a dimensionless form for the purpose of generality to the suggested optimization of the bearing profile, as explained previously.

Table 2 shows the effects of shaft axis deviation (misalignment) on the main bearing characteristics in their dimensionless forms, which are maximum pressure (P_o), minimum film thickness (H_o), and the coefficient of friction (f). The dimensionless misalignment parameters are $\Delta h_o = 0.56$ and $\Delta v_o = 0.56$, which are selected to have sever negative effects on bearing performance. This table also illustrates corresponding results for the aligned case. The deviation in the shaft axis has very clear negative impacts on these characteristics. The increase in P_o is 35.55 %, and more importantly, the reduction in the minimum film thickness is 79.50%. Furthermore, the friction coefficient is also increased by 11.7%. These effects will certainly affect the general performance of the bearing in terms of load-carrying capacity, reliability of the system, and bearing life. Therefore, any possible improvement in these characteristics represents a significant step toward obtaining a sufficient bearing design and increasing the rotor-bearing system’s reliability.

Table 2. Effects of shaft axis deviation on the maximum pressure, minimum film thickness, and friction coefficient (dimensionless values).

	Aligned	Misaligned	% Change
P_o	0.6444	0.8735	+35.55
H_o	0.4	0.0820	−79.50
f	2.2178	2.4656	+11.17

Owing to the importance of film thickness, contact pressure, and the coefficient of friction, which reflect the level of performance of the bearings, a detailed investigation is required to overcome the problem of shaft deviation. This investigation should consider the compound effects of these factors to evaluate the performance of the bearing. This will be very useful for finding and introducing optimal design parameters based on the weighted sum model (WSM), which can be written as [45]

$$A_i^{WSM-Score} = \sum_{j=1}^n w_j a_{ij}, \quad \text{for } i = 1, 2, 3 \dots, m \tag{19}$$

where w_j and a_{ij} are the relative weight and performance value of each factor, respectively. The relative weight value for each factor affecting the performance of the bearing is chosen according to its importance. A relative weight of 50% is chosen for film thickness, while the relative weights for both pressure and friction are chosen equally with a value of 25%. This decision is made based on more than 15 years of experience in this field. Table 3 presents the results and performance values of each factor (pressure, film thickness, and friction coefficient) across nine runs. The details of these nine runs will be explained later.

Table 3. The results and performance values of pressure, film thickness, and friction.

Run No.	P_o	$P_o (-)$	H_o	$H_o (-)$	f	$f (-)$
1	0.8449	0.864599	0.0947	0.311411	2.4542	0.864029
2	0.7706	0.947963	0.2384	0.783953	2.2611	0.937818
3	2.6278	0.277989	0.0839	0.275896	2.1205	1
4	0.7539	0.968961	0.1628	0.53535	2.3843	0.88936
5	0.7954	0.918406	0.3041	1	2.2147	0.957466
6	0.8346	0.87527	0.0912	0.299901	2.4276	0.873496
7	0.7305	1	0.1591	0.523183	2.3671	0.895822
8	0.8434	0.866137	0.0935	0.307465	2.4492	0.865793
9	0.7963	0.917368	0.1996	0.656363	2.2766	0.931433

The Taguchi L-9 orthogonal array is used to select the minimum number of numerical cases that contain different combinations of the design factors to provide significant results about the effect of these factors on the performance of the system. So, it is considered a valuable tool in numerical analysis for evaluating the effects of multiple parameters on a computational model, with minimal resources and time investment. Another reason for selecting the Taguchi method is to systematically investigate how different combinations of input parameters influence the numerical results and which combinations leads to more stable and accurate outcomes. Furthermore, the results of the Taguchi method provide a better understanding on how different parameters interact and their effect on numerical analysis, which can be valuable in refining models and improving accuracy.

Table 4 presents the parameters and the weighted sum model using the Taguchi L-9 orthogonal array. The results show that the best outcome ($WSM = 0.968$) is obtained in run 5, which contains relatively optimal values for minimum film thickness (H_o), maximum pressure (P_o), and coefficient of friction (f). On the other hand, the worst results are obtained in run 3 ($WSM = 0.457$), where the lowest value of H_o and the highest values of P_o and f have occurred.

Table 4. The parameters and the Taguchi L-9 orthogonal array results.

Taguchi Method for Modified Bearing ($L/D=1.25$)				
No. of Run	Parameters			WSM
	n	ζ	ψ	
1	1 (1)	1 (0.1)	1 (0.01)	0.587862
2	1 (1)	2 (0.4)	2 (0.2)	0.863421
3	1 (1)	3 (1.0)	3 (0.4)	0.457445
4	2 (2)	1 (0.1)	2 (0.2)	0.732255
5	2 (2)	2 (0.4)	3 (0.4)	0.968968
6	2 (2)	3 (1.0)	1 (0.01)	0.587142
7	3 (3)	1 (0.1)	3 (0.4)	0.735547
8	3 (3)	2 (0.4)	1 (0.01)	0.586715
9	3 (3)	3 (1.0)	2 (0.2)	0.790382

Figure 6 shows the main effects plot for means, where the dotted line denotes the mean of means for all the results (the average of 9 WSM readings). The blue points represent the mean of three results for each parameter level. Figure 7 represents the main effect of signal-to-noise (S/N) ratios against the low, medium, and high (L , M , and H) levels of n , ζ , and ψ .

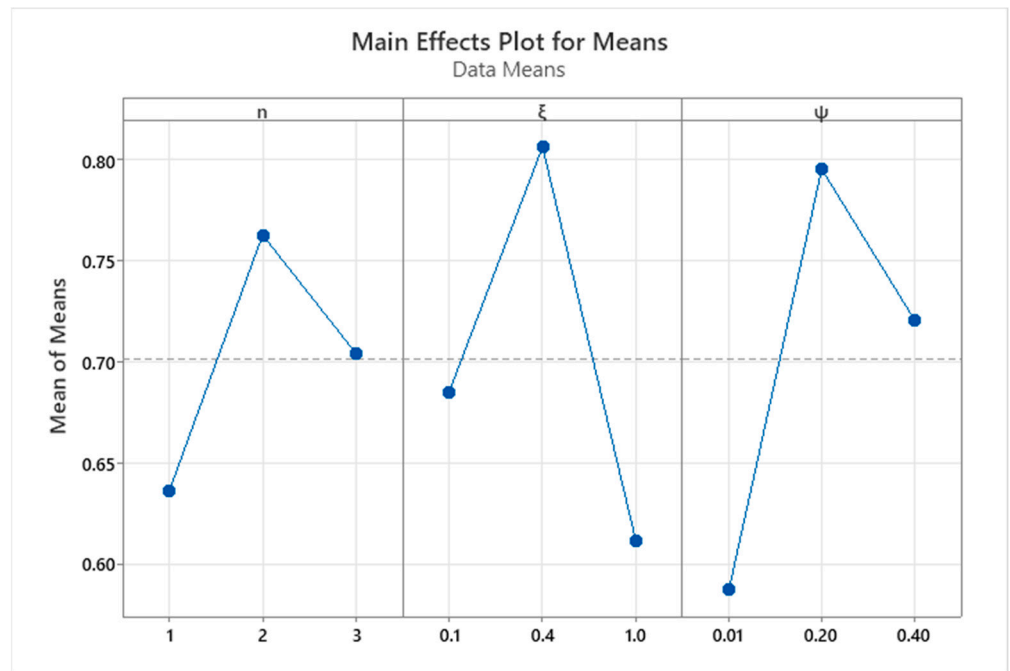


Figure 6. The main effects plot for means of the selected parameters. $n = 1$: linear, $n = 2$: quadratic and $n = 3$: cubic profile; ξ and ψ are the design parameters in the radial and longitudinal directions, respectively.

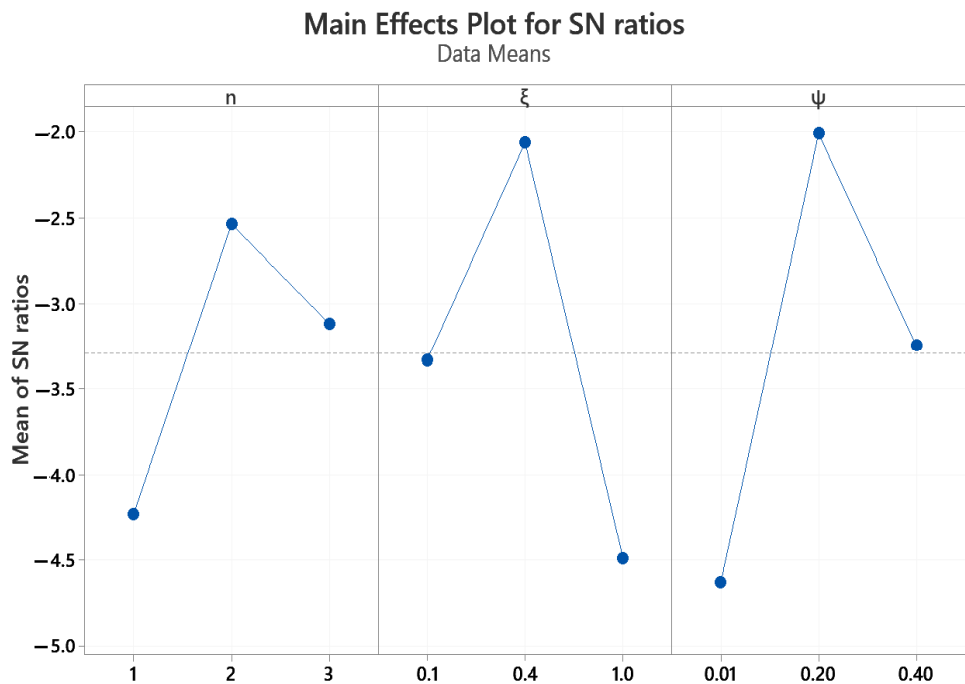


Figure 7. The main effects plot for S/N ratios.

Figures 8–10 show the WORKSHEET Contour Plots of WSM vs. ξ and ψ , WSM vs. n and ψ , and WSM vs. n and ξ , respectively. The examination of these figures (Figures 6–10) clearly illustrates that the optimal geometrical parameters for the bearing profile are $n = 2$, $\xi = 0.4$, and $\psi = 0.2$. The effect of these values on the considered characteristics will be illustrated in detail in the following paragraphs.

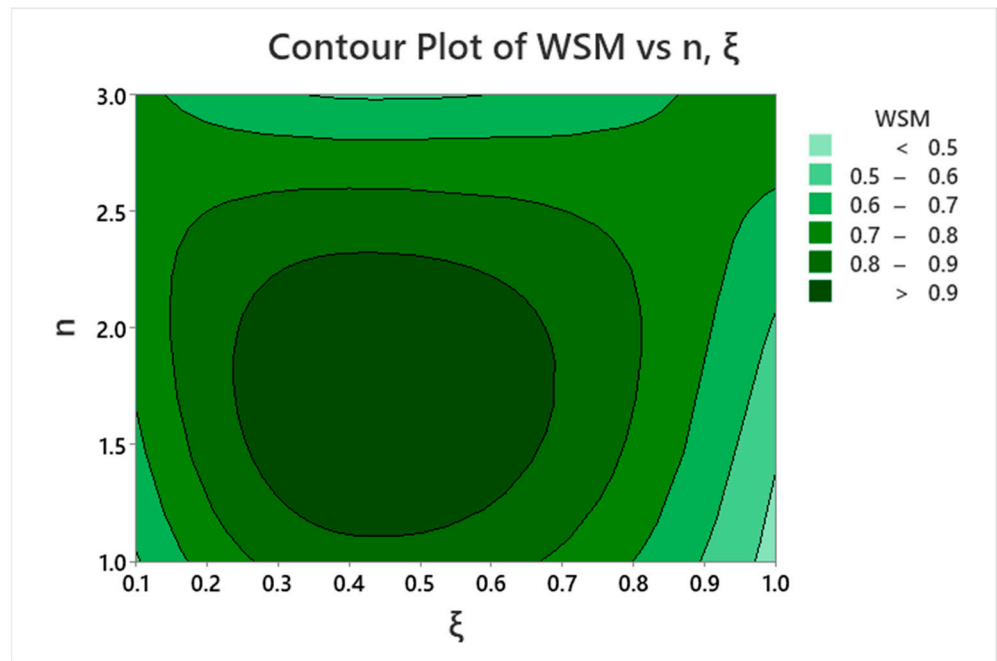


Figure 8. Contour plot of WSM with respect to n and ξ .

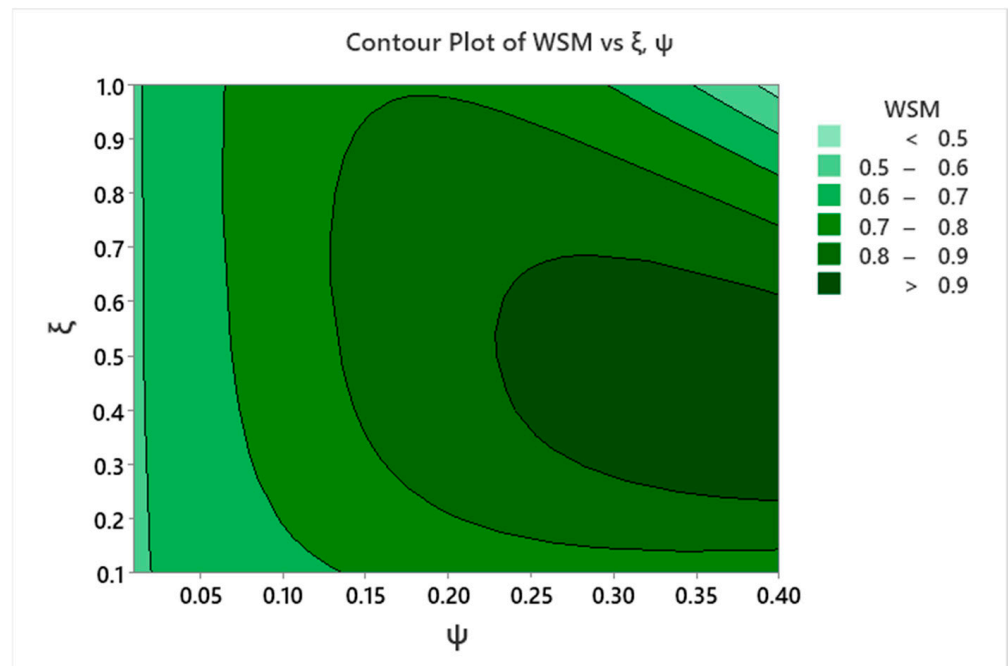


Figure 9. Contour plot of WSM with respect to ξ and ψ .

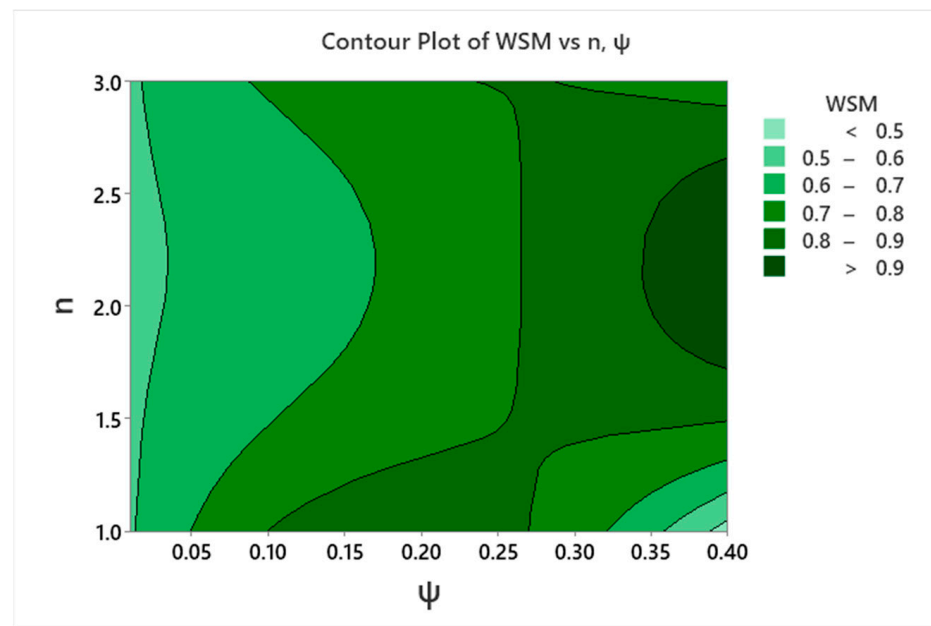


Figure 10. Contour plot of WSM with respect to n and ψ .

Table 5 shows the effect of using the modification data from the Taguchi method. The curve order is 2, and the profile parameters are $\zeta = 0.4$ and $\psi = 0.2$. It can be seen that the suggested profile reduces P_o by 15.08%, increases H_o by 183.9%, and also reduces the friction coefficient by 6.36%. These are very important outcomes, as the bearing can operate safely if the profile is modified on both sides of the bearing, despite working under such severe misalignment conditions. The most important outcome for the results presented in this table is the improvement in the minimum film thickness (almost doubled) due to the profile modification, as it was severely thinned due to misalignment. More improvements due to profile modification will be illustrated later in terms of the distribution shapes.

Table 5. Effects of bearing profile optimization on maximum pressure, minimum film thickness, and friction coefficient undershaft axis deviation. $n = 2, \zeta = 0.4, \psi = 0.2$.

	Misaligned	Modified	% Change
P_o	0.8735	0.7418	−15.08
H_o	0.0820	0.2328	+183.90
f	2.4656	2.3089	−6.36

Figure 11 shows the shape of the resulting pressure and film thickness distributions due to profile modification compared to the aligned and misaligned cases. The pressure distributions are shown on the left side, while the corresponding film thickness distributions are illustrated on the right side. The results of the modified case are the suggested optimal profile parameter values from the Taguchi method ($n = 2, \zeta = 0.4,$ and $\psi = 0.2$). Figure 11a shows the shapes of the pressure and film thickness distributions for the aligned case. It is clear that the pressure is symmetrical along the middle of the bearing length, and the film thickness extends along the bearing length. However, as previously explained, this ideal situation does not exist in real industrial applications of journal bearings due to unavoidable misalignment. Figure 11b shows the corresponding results for the aligned case, where both distributions are no longer symmetric (about $Z = 1/2$). Such distributions have a clear effect on the generation of obvious pressure spikes and the thinning of film thickness at the edges of the bearing. Furthermore, this loss of symmetry shifts the point of equivalent load away from the middle of the bearing width, which may affect the dynamic behavior of the bearing under external, time-varying excitations. These consequences

are clearly reduced in the distributions shown in Figure 10c, where the bearing profile is modified. The distribution of the pressure is more uniform, and the film thickness levels are elevated on both sides of the bearing (close to $Z = 0$ and $Z = 1$).

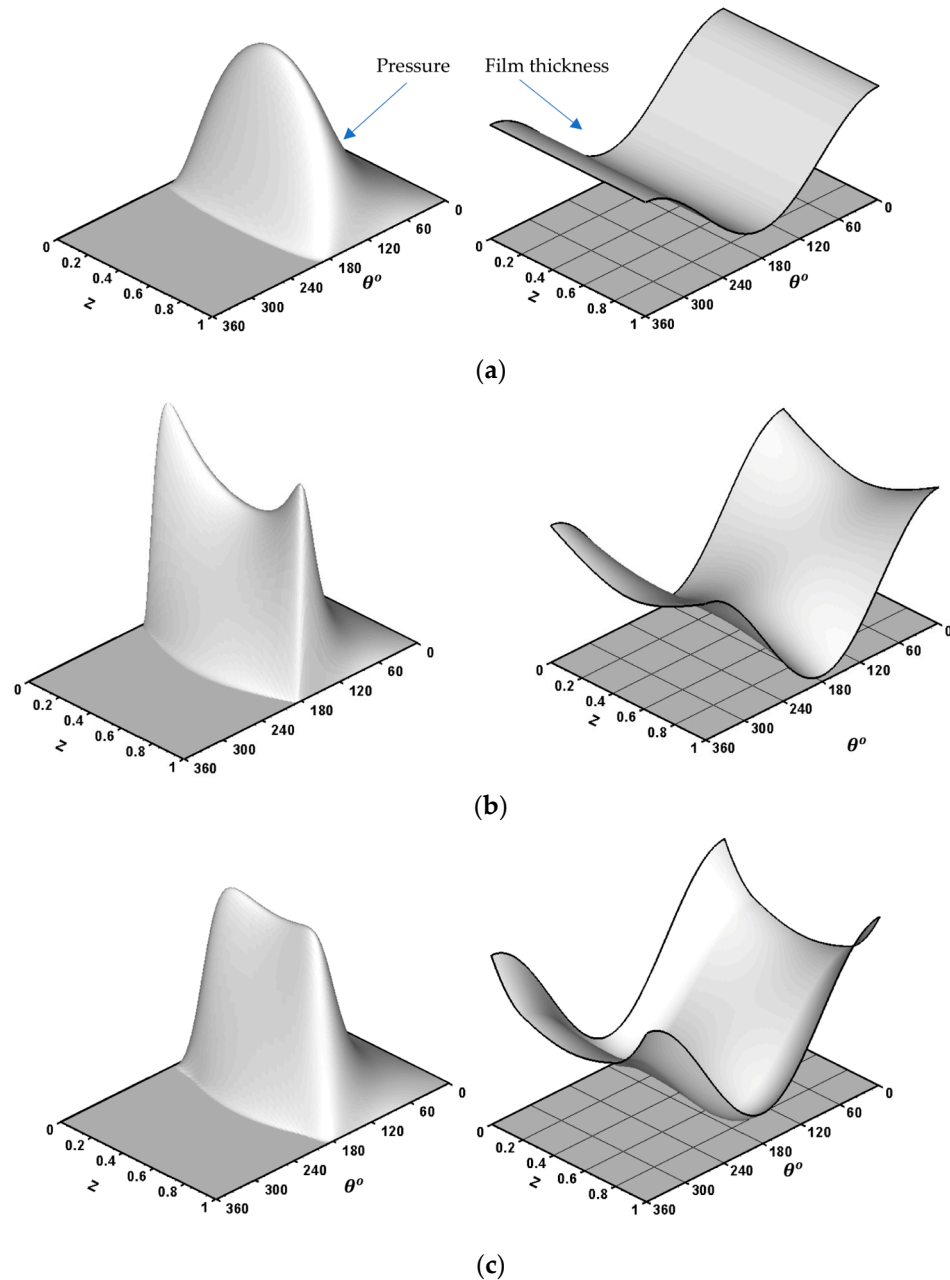


Figure 11. Shape of pressure (left) and film thickness (right) distributions. (a) Ideal case, (b) shaft deviation and (c) optimized profile.

More relevant details about the results illustrated in this figure (Figure 10) are shown in Figures 12 and 13. Figure 12 shows side views (bearing width side) of the pressure distribution for the aligned, misaligned, and optimized profile. It can be seen how the modification reduces the pressure values and produces an acceptable distribution of the pressure in comparison with the misaligned case. The side views (circumferential direction) of the film thickness distributions are shown in Figure 13. The arrows in this figure point to the minimum film thickness positions for the three cases. This figure clearly shows the extent to which misalignment places the bearing system in unsafe operating conditions and how the modification of the bearing profile is important in elevating film thickness levels.

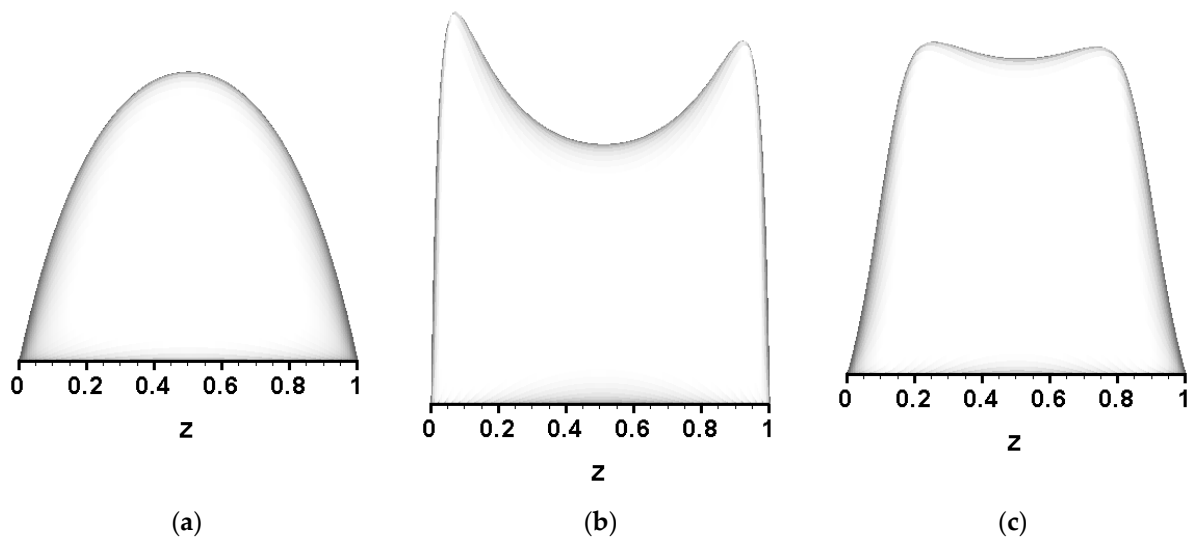


Figure 12. Side view of the pressure distributions. (a) Ideal, (b) misaligned and (c) optimized.

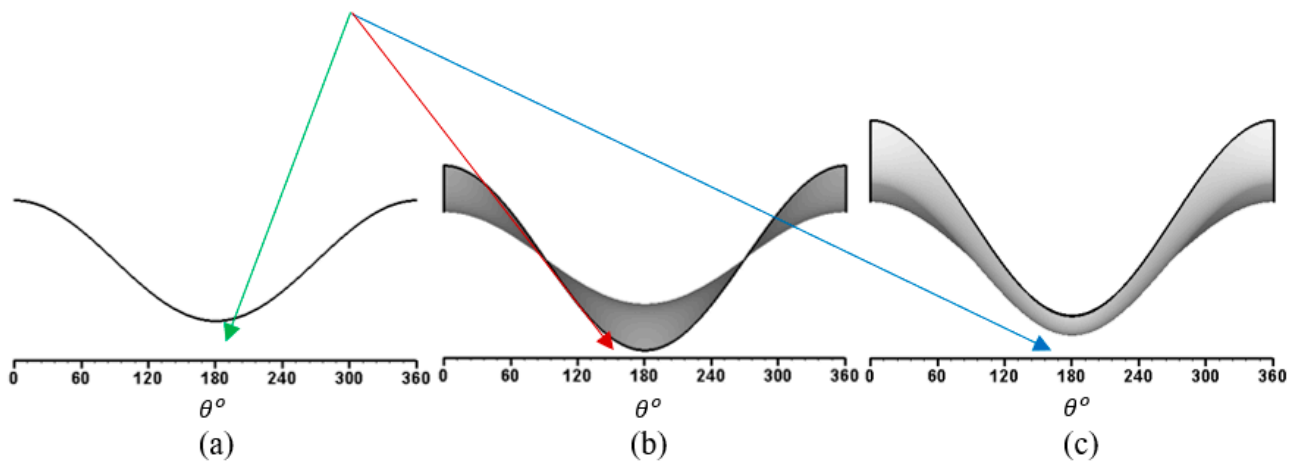


Figure 13. Side view of the film thickness distributions. (a) Ideal, (b) misaligned and (c) optimized.

Further comparisons among the results for the three cases (aligned, misaligned, and modified bearing) are shown in Figure 14. This figure illustrates a sectional comparison at $\theta = 180^\circ$ along the bearing width. It is worth mentioning that the film thickness is at its minimum value at this section in the aligned case. Figure 14a shows this comparison for the ideal case where the pressure is clearly symmetric, with a consistent film thickness over the whole length of the bearing. Figure 14b shows the corresponding comparison for the misaligned case, where the thickness of the lubricant is significantly disturbed along the bearing width. The pressure curve also differs from the corresponding aligned curve, which emphasizes that misalignment causes an overall change in pressure distribution, not only in positions where the gap between the surfaces is reduced. It is worth mentioning that the maximum pressure occurs at different sections (at a section of $\theta \neq 180^\circ$). The last figure (Figure 14c) clearly illustrates how the modification is necessary in terms of increasing film thickness values in positions where shaft deviation has its most negative impact.

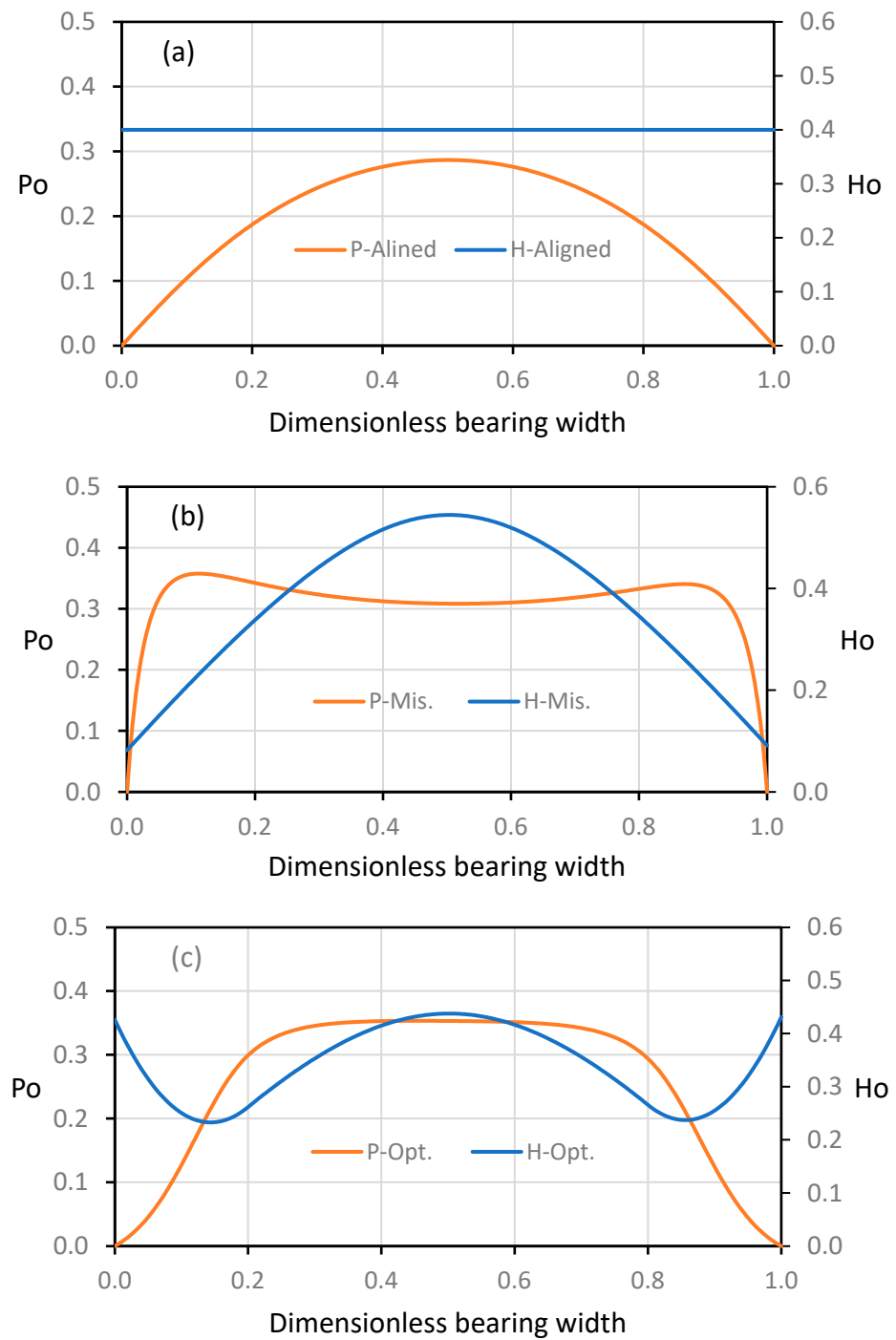


Figure 14. Variations in dimensionless pressure and dimensionless film thickness along the bearing width at $\theta = 180^\circ$. (a) Ideal, (b) misaligned and (c) optimized profile case.

The following bearing and lubricant characteristics are used to obtain results in dimensional form: bearing width = 80 mm, diameter = 64 mm, clearance = 0.1175 mm, eccentricity = 0.6, rotational speed = 3000 rpm, and oil viscosity = 0.0293 Pa.s. These parameters are taken from [29], except for the eccentricity ratio and the bearing diameter, which were selected to obtain an L/D ratio of 1.25 in order to be consistent with the value considered in the current work. The misalignment parameters are 0.56, and the modification parameters are $n = 2$, $\zeta = 0.4$, and $\psi = 0.2$. Table 6 shows the results in SI units, demonstrating how the optimized profile improves the level of minimum film thickness and reduces the maximum pressure value.

Table 6. Results of the optimized design in a dimensional form.

Characteristic	Unit	Ideal Case	Under Shaft Deviation	Optimized Design Under Shaft Deviation	% Change (4th and 5th Column)
Min. film thickness	μm	47.000	9.635	27.354	+183.90
Max. Pressure	MPa	2.63966	3.57813	3.03864	−15.08

5. Conclusions

This work uses the Taguchi method to investigate bearing design under the influence of severe shaft deviation conditions with respect to the bearing's longitudinal axis. The L-9 orthogonal array of the Taguchi method is used in this analysis, where three parameters are considered, and each parameter consists of three levels. The three parameters are the order of the profile (n), the position of the modification along the bearing width (ψ), and the amount of modification (ζ) in the radial direction. The three levels of the bearing profiles are linear, quadratic, and cubic. A general shaft deviation model is considered in order to simulate deviations in the horizontal and vertical planes, which are incorporated in the numerical solution using the finite difference method. The solution of the Taguchi method considers the compound effect of three main bearing characteristics (minimum film thickness, maximum pressure, and coefficient of friction) based on the use of a weighted sum model, as investigating a single characteristic does not provide an actual evaluation of the bearing modification. The results show that shaft deviation increases the maximum pressure by 35.6% and decreases the minimum film thickness and friction coefficient by 79.5% (from 0.4 to 0.0820) and 11.2%, respectively. Using the suggested profiles and optimizing the results with the Taguchi method shows that the use of $n = 2$, $\zeta = 0.4$, and $\psi = 0.2$ significantly enhances the bearing performance, despite the presence of severe levels of shaft deviation. The most important outcome is the almost 184% increase in the minimum film thickness (from 0.0820 to 0.2328) in comparison to the corresponding misaligned value. This increase in film thickness is also accompanied by 15.1% and 6.4% reductions in the maximum pressure and friction coefficient, respectively. Further investigations are required to consider the corresponding effects on the dynamic response of the system.

Author Contributions: Methodology, Investigation, Writing—Review and Editing—Funding Acquisition, Resources, H.U.J. and M.N.M.; Validation, Funding Acquisition, Resources, H.S.S.A.; Formal Analysis, Funding Acquisition, Resources, M.J.J.; Investigation, Project Administration, Writing—Review and Editing, O.I.A. All authors have read and agreed to the published version of the manuscript.

Funding: This research received no external funding.

Data Availability Statement: The study did not report any data.

Conflicts of Interest: The authors declare no conflict of interest.

References

- Jeon, W.-J.; Hong, S.-H. A New Type of Misaligned Journal Bearing with Flexible Structure. *Lubricants* **2023**, *11*, 256. [CrossRef]
- Du, F.; Li, D.; Sa, X.; Li, C.; Yu, Y.; Li, C.; Wang, J.; Wang, W. Overview of Friction and Wear Performance of Sliding Bearings. *Coatings* **2022**, *12*, 1303. [CrossRef]
- Huang, Y.; Cao, H.; Tian, Z. Stability analysis of long hydrodynamic journal bearings based on the journal center trajectory. *Friction* **2021**, *9*, 1776–1783. [CrossRef]
- Ebrat, O.; Mourelatos, Z.P.; Vlahopoulos, N.; Vaidyanathan, K. Calculation of Journal Bearing Dynamic Characteristics Including Journal Misalignment and Bearing Structural Deformation[®]. *Tribol. Trans.* **2004**, *47*, 94–102. [CrossRef]
- Jamali, H.U.; Al-Hamood, A. A New Method for the Analysis of Misaligned Journal Bearing. *Tribol. Ind.* **2018**, *40*, 213–224. [CrossRef]
- Das, S.; Guha, S.K.; Chattopadhyay, A.K. On the steady-state performance of misaligned hydrodynamic journal bearings lubricated with micropolar fluids. *Tribol. Int.* **2002**, *35*, 201–210. [CrossRef]
- Zhang, Z.S.; Dai, X.D.; Zhang, Z.N.; Xie, Y.B. Thermoelastohydrodynamic behavior of misaligned plain journal bearings. *Proc. Inst. Mech. Eng. Part C J. Mech. Eng. Sci.* **2013**, *227*, 2582–2599. [CrossRef]

8. Zheng, L.; Zhu, H.; Zhu, J.; Deng, Y. Effects of oil film thickness and viscosity on the performance of misaligned journal bearings with couple stress lubricants. *Tribol. Int.* **2020**, *146*, 106229. [[CrossRef](#)]
9. Murawski, I. Shaft line whirling vibrations: Effects of numerical assumptions on analysis results. *Mar. Technol.* **2005**, *42*, 53–60. [[CrossRef](#)]
10. Lv, F.; Ta, N.; Rao, Z. Analysis of equivalent supporting point location and carrying capacity of misaligned journal bearing. *Tribol. Int.* **2017**, *116*, 26–38. [[CrossRef](#)]
11. Jang, J.Y.; Khonsari, M.M. On the characteristics of misaligned journal bearing. *Lubricants* **2015**, *3*, 27–53. [[CrossRef](#)]
12. Pigott, R.J.S. Bearings and lubricant-bearing troubles traceable to design can be avoided by engineering study. *Mech. Eng.* **1942**, *64*, 259–269.
13. Sun, J.; Gui, C. Hydrodynamic lubrication analysis of journal bearing considering misalignment caused by shaft deformation. *Tribol. Int.* **2004**, *37*, 841–848. [[CrossRef](#)]
14. Sun, J.; Gui, C.; Li, Z. An experimental study of journal bearing lubrication effected by journal bearing misalignment as a result of shaft deformation under load. *J. Tribol.* **2005**, *127*, 813–819. [[CrossRef](#)]
15. Etsion, I.; Gomed, K. Improved design with noncylindrical profiles of gas-lubricated ringless pistons. *J. Tribol.* **1995**, *117*, 143–147. [[CrossRef](#)]
16. Nikolakopoulos, P.G.; Papadoulos, C.A. A study of friction in worn misaligned journal bearings under severe hydrodynamic lubrication. *Tribol. Int.* **2008**, *41*, 461–472. [[CrossRef](#)]
17. Song, X.; Wu, W.; Yuan, S. Mixed-lubrication analysis of misaligned journal bearing considering turbulence and cavitation. *AIP Adv.* **2022**, *12*, 015213. [[CrossRef](#)]
18. Shenoy, S.B.; Pai, R. Theoretical investigations on the performance of an externally adjustable fluid-film bearing including misalignment and turbulence effects. *Tribol. Int.* **2009**, *42*, 1088–1100. [[CrossRef](#)]
19. Ram, N.; Sharma, S.C. Influence of wear on the performance of hole-entry hybrid misaligned journal bearing in turbulent regime. *Ind. Lubr. Tribol.* **2014**, *66*, 509–519. [[CrossRef](#)]
20. Ram, N.; Sharma, S.C. A study of misaligned hole-entry worn journal bearing operating in turbulent regime. *Ind. Lubr. Tribol.* **2013**, *65*, 108–118. [[CrossRef](#)]
21. Muskat, M.; Morgan, F. Studies in lubrication V. The theory of the thick film lubrication of flooded journal bearings and bearings with circumferential grooves. *J. Appl. Phys.* **1939**, *10*, 398–407. [[CrossRef](#)]
22. Dufrane, K.F.; Kannel, J.W.; McCloskey, T.H. Wear of steam turbine journal bearings at low operating speeds. *J. Lubr. Technol.* **1983**, *105*, 313–317. [[CrossRef](#)]
23. Strzelecki, S. Operating Characteristics of Heavy Loaded Cylindrical Journal Bearing with Variable Axial Profile. *Mater. Res.* **2005**, *8*, 481–486. [[CrossRef](#)]
24. Nacy, S.M. Effect of Chamfering on Side-Leakage Flow Rate of Journal Bearings. *Wear* **1997**, *212*, 95–102. [[CrossRef](#)]
25. Fillon, M.; Bouyer, J. Thermohydrodynamic Analysis of a Worn Plain Journal Bearing. *Tribol. Int.* **2004**, *37*, 129–136. [[CrossRef](#)]
26. Chasalevris, A.; Dohnal, F. Enhancing Stability of Industrial Turbines Using Adjustable Partial Arc Bearings. *J. Phys.* **2016**, *744*, 012152. [[CrossRef](#)]
27. Ren, P.; Zuo, Z.; Huang, W. Effects of axial profile on the main bearing performance of internal combustion engine and its optimization using multiobjective optimization algorithms. *J. Mech. Sci. Technol.* **2021**, *35*, 3519–3531. [[CrossRef](#)]
28. Bouyer, J.; Fillon, M. Improvement of the THD Performance of a Misaligned Plain Journal Bearing. *ASME J. Tribol.* **2003**, *125*, 334–342. [[CrossRef](#)]
29. Liu, C.; Li, W.; Lu, X.; Zhao, B. Effects of double parabolic profiles with groove textures on the hydrodynamic lubrication performance of journal bearing under steady operating conditions. *Mech. Ind.* **2020**, *21*, 301. [[CrossRef](#)]
30. Hagemann, T.; Ding, H.; Radtke, E.; Schwarze, H. Operating Behavior of Sliding Planet Gear Bearings for Wind Turbine Gearbox Applications—Part I: Basic Relations. *Lubricants* **2021**, *9*, 97. [[CrossRef](#)]
31. Jia, D.; Li, C.; Deng, W.; Ji, H.; Hao, L. Effects of Hyperelliptic Bearings Bush on Connecting Rod Big-End Lubrication and Design Optimization. *Lubricants* **2023**, *11*, 293. [[CrossRef](#)]
32. Jamali, H.U.; Sultan, H.S.; Abdullah, O.I.; Al-Tamimi, A.N.J.; Abbud, L.H.; Ruggiero, A.; Al-Dujaili, Z.A. Effect of Chamfer Form and Parameters on the Characteristics of Finite Length Journal Bearing under Impact Load. *Lubricants* **2023**, *11*, 73. [[CrossRef](#)]
33. Ganesha, A.; Joseph, A.; Pai, R.; Khader, S.M.A.; Kumar, N.; Kumar, S.; Girish, H. Performance Optimization of a Multi-groove Water Lubricated Journal Bearing with Partial Slip by Taguchi Analysis. *Arab. J. Sci. Eng.* **2023**. [[CrossRef](#)]
34. Yücel, E.; Saruhan, H. Design optimization of rotor-bearing system considering critical speed using Taguchi method. *Proc. Inst. Mech. Eng. Part E J. Process Mech. Eng.* **2017**, *231*, 138–146. [[CrossRef](#)]
35. Chen, C.-Y.; Liu, C.-S.; Tee, C.-K.; Li, Y.-C. Application of stabilized term in free boundary problems for optimizing bi-directional-rotation herringbone-grooved journal bearings. *Appl. Math. Model.* **2017**, *47*, 826–838. [[CrossRef](#)]
36. Sharma, V.; Singh, R.; Chaudhary, R. *Experimental Study of Sliding Wear Behavior of the Casted Lead Bronze Journal Bearing Material*; SAE Technical Paper 2019-01-0824; SAE International: Warrendale, PA, USA, 2019. [[CrossRef](#)]
37. Chen, C.; Liu, C.; Li, Y.; Mou, S. Geometry optimization for asymmetrical herringbone grooves of miniature hydrodynamic journal bearings by using Taguchi technique. *Proc. Inst. Mech. Eng. Part J J. Eng. Tribol.* **2015**, *229*, 196–206. [[CrossRef](#)]
38. Bhasker, B.; Seetharamaiah, N.; Babu, P.R.; Gugulothu, S.K. A novel assessment study on a dynamic analysis of hydrodynamic journal bearing performance: A Taguchi-fuzzy based approach optimization. *Transp. Eng.* **2020**, *2*, 100033. [[CrossRef](#)]

39. Chasalevris, A.; Sfyris, D. Evaluation of the Finite Journal Bearing Characteristics, Using the Exact Analytical Solution of the Reynolds Equation. *Tribol. Int.* **2013**, *57*, 216–234. [[CrossRef](#)]
40. Hamrock, B.J. *Fundamentals of Fluid Film Lubrication*; McGraw-Hill, Inc.: New York, NY, USA, 1991. [[CrossRef](#)]
41. Harnoy, A. *Bearing Design in Machinery: Engineering Tribology and Lubrication*, 1st ed.; Marcel Dekker Inc.: New York, NY, USA; Basel, Switzerland, 2002. [[CrossRef](#)]
42. Vijayaraghavan, D.; Keith, T.G. Analysis of a Finite Grooved Misaligned Journal Bearing Considering Cavitation and Starvation Effects. *ASME J. Tribol.* **1990**, *112*, 60–67. [[CrossRef](#)]
43. Feng, H.; Jiang, S.; Ji, A. Investigation of the Static and Dynamic Characteristics of Water-Lubricated Hydrodynamic Journal Bearing Considering Turbulent, Thermo-hydrodynamic and Misaligned Effects. *Tribol. Int.* **2019**, *130*, 245–260. [[CrossRef](#)]
44. Lund, J.W.; Thomsen, K.K. A Calculation Method and Data for the Dynamic Coefficients of Oil-Lubricated Journal Bearings. In *Topics in Fluid Film Bearing and Rotor Bearing System Design and Optimization*; ASME: New York, NY, USA, 1978.
45. Fishburn, P.C. Additive Utilities with Incomplete Product Set: Applications to Priorities and Assignments. *J. Oper. Res. Soc. Am.* **1967**, *15*, 373–589. [[CrossRef](#)]

Disclaimer/Publisher’s Note: The statements, opinions and data contained in all publications are solely those of the individual author(s) and contributor(s) and not of MDPI and/or the editor(s). MDPI and/or the editor(s) disclaim responsibility for any injury to people or property resulting from any ideas, methods, instructions or products referred to in the content.